

Underlying Mechanism of Inkjet Printing of Uniform Organic Semiconductor Films Through Antisolvent Crystallization

Yuki Noda,* Hiromi Minemawari, Hiroyuki Matsui, Toshikazu Yamada, Shunto Arai, Tadashi Kajiya, Masao Doi, and Tatsuo Hasegawa*

An underlying mechanism is reported for the formation of highly uniform crystalline organic semiconductor films by the double-shot inkjet printing (IJP) technique utilizing antisolvent crystallization. It is demonstrated that the ability to form uniform films with this technique can be attributed to the unique nature of the initial contact dynamics between the chemically different microdroplets before occurrence of solute crystallization. Experiments are conducted systematically where a single microdroplet is over-deposited by the IJP technique on a chemically different sessile droplet, for ten kinds of pure and miscible solvent combinations. The subsequent behavior is observed by high speed camera. The initial contact dynamics can be classified into three dramatically different cases that are respectively referred to as wetting, dewetting, and sinking. These phenomena are unique to microdroplets and the conditions for the occurrence of each type of phenomenon can be consistently explained by the fact that the initial contact dynamics are driven by the difference of surface tension of the liquids. Among the three kinds of dynamics, the wetting phenomenon creates a thin solution layer on the antisolvent droplet surface and can be used thus to manufacture uniform semiconductor films, where the coffee ring effect can be eliminated.

1. Introduction

Inkjet printing (IJP) is a unique technology that can produce, allocate, and deposit microdroplets, with a volume ranging between 100 pL and 1 fL, on paper or substrates. IJP has attracted considerable attention recently as a novel print production technology of electronic devices,^[1–4] referred to as “printed electronics,” with the aim of manufacturing large-area and flexible electronic devices.^[5,6] Because it is now possible to utilize commercially available inkjet printers to print documents or photo images on paper with a spatial resolution higher than 1200 × 1200 dpi, it appears auspiciously easy to manufacture electronic devices with a similar high pattern resolution. However, there is a crucial difference between document printing and production of electronic devices. In order to power electronic devices, it is necessary to form and stack uniform patterned layers of electronic functional materials at atomic

or molecular scales on flat substrate surfaces. Solving this issue is quite difficult with conventional IJP processes, mainly because of the existence of characteristic fluid flow dynamics due to solvent evaporation from the deposited microdroplets. A particular case in point is the coffee-ring effect which is caused by an outward capillary flow generated by solvent evaporation that carries solutes toward the contact line of microdroplets.^[7–9] Several efforts have been made up to now to overcome such an undesired distribution of the deposits by adding surfactants,^[10,11] exposing to solvent vapor,^[12] or changing the shape of the suspended particles,^[13] substrate temperature,^[14] or acidity of solution,^[15] although these attempts have not proved successful in improving device characteristics.

Recently, it was reported^[16] that when antisolvent crystallization, i.e., a binary liquid mixture of a material solution and an antisolvent, is incorporated into an IJP-based microdroplet process, it becomes possible to manufacture highly uniform thin films as precipitates, where the coffee-ring effect can be eliminated. It was expected that the use of antisolvent crystallization could separate the time of occurrence of the solute crystallization and the solvent evaporation. However, it was also observed that the semiconductor thin films grew around the

Dr. Y. Noda, Dr. H. Minemawari, Dr. T. Yamada,
Prof. T. Hasegawa
National Institute of Advanced Industrial
Science and Technology (AIST)
AIST Tsukuba Central 4, 1-1-1 Higashi,
Tsukuba 305-8562, Japan
E-mail: y-noda@aist.go.jp, yuki.n.noda@gmail.com
t-hasegawa@ap.t.u-tokyo.ac.jp



Dr. H. Matsui
Department of Advanced Materials Science
University of Tokyo
5-1-5 Kashiwanoha, Kashiwa 277-8561, Japan

Dr. S. Arai, Dr. T. Kajiya, Prof. T. Hasegawa
Department of Applied Physics
The University of Tokyo
7-3-1 Hongo, Tokyo 113-8656, Japan

Dr. T. Kajiya
Max Planck Institute for Polymer Research
Ackermannweg 10, 55128 Mainz, Germany

Prof. M. Doi
Interdisciplinary Research Center
Beihang University
100191 Beijing, China

DOI: 10.1002/adfm.201500802

liquid–air interfaces of the mixed droplets. By taking advantage of this feature, it was also demonstrated that single-crystalline films can be grown by an elaborately shaped sessile antisolvent droplet produced via modification of the substrate surfaces. It is to be noted that this feature is in striking contrast to conventional macroscopic antisolvent crystallization that produces a large mass of microcrystals due to rapid turbulent mixing.^[17] It is quite likely that the chemically different binary microdroplet will exhibit unique mixing phenomena essentially different from macroscale fluids, although such mixing dynamics has not yet been reported.

Concerning the unique nature of microdroplets, it has been pointed out that the surface (or interfacial) tension is predominant, primarily due to the high surface-area-to-volume ratio of the microdroplets.^[18] It is thus expected that the mixing dynamics of the microdroplets should be considerably affected by the difference in surface tension between the mixed liquids. Karpitschka and Riegler^[19] observed that when two chemically different sessile droplets come within close contact of each other, they do not coalesce immediately but remain separated in a temporary state of noncoalescence. Based on hydrodynamic analyses of the phenomenon, Borgia and Bestehorn^[20] deliberated that the surface tension gradient causes Marangoni flow at the neck region where the two droplets are connected, eventually producing a temporary dewetting of states between the two droplets. Yerushalmi-Rozen et al.^[21] also reported that mixtures composed of two kinds of oligomers on a solid surface undergo phase separation which is driven by the difference in surface tension. However, the mixing dynamics in which a microdroplet is over-deposited on a chemically different sessile droplet and their effect on the IJP-based antisolvent crystallization process have not yet been studied.

In this work, we first investigated by means of high-speed camera microscope observations how chemically different microdroplets come into contact and start mixing with each other, in the situation where the microdroplet is over-deposited on a chemically different sessile droplet on a solid surface (Figure 1). We systematically conducted these experiments for ten kinds of pure solvent combinations that are miscible with each other in equilibrium, but possess different density, polarity, and surface tension values. Consequently, we observed that three kinds of initial contact dynamics appear within the time scale before molecular mixing takes place by diffusion and that the appearance of each phenomenon depends on the droplet volume and solvent combinations. In this paper, we discuss the disparity in these phenomena with regards to the variation in total surface energy caused by the transformation in shape of both the over-deposited microdroplet and the sessile

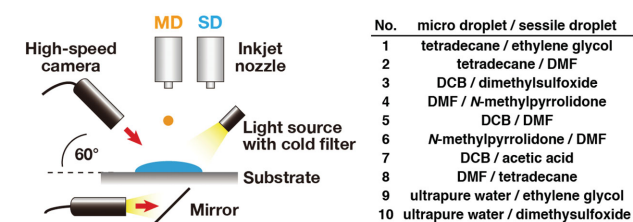


Figure 1. Schematic of the experimental setup and a list of the ten miscible liquid combinations of microdroplet and sessile droplet.

droplet induced by an instantaneous advection flow just after the contacts. We then proceed to present and discuss how uniform thin film growth is achieved when organic semiconductor solution and antisolvent are used as the over-deposited droplet and the sessile droplet, respectively. It is demonstrated that growth of uniform crystalline films clearly depends on the initial contact dynamics of the microdroplets.

2. Results and Discussion

2.1. Observation of Initial Contact Dynamics of Microdroplets

In Figure 2, the size effect as observed for the droplet mixing dynamics is shown in time-lapse images after deposition of 1,2-dichlorobenzene (DCB) droplet a) by a micropipette ($\approx 20 \mu\text{L}$), b) an inkjet head ($\approx 1.5 \text{ nL}$), and c) the other inkjet head (0.6 nL) on a surface of *N,N*-dimethylformamide (DMF). When the volume of the deposited droplet is a) $20 \mu\text{L}$, the initial contact dynamics is governed by a sinking of the deposited droplet due to the density difference (or gravitation), followed by a gradual turbulent or diffusion mixing inside the sessile droplet. By contrast, when the volume of the deposited droplet is c) 0.6 nL , the initial contact dynamics present quite different behavior, where the deposited microdroplet is instantaneously deformed and spreads over the liquid surface without exhibiting turbulence. The deposition when the volume b) is 1.5 nL

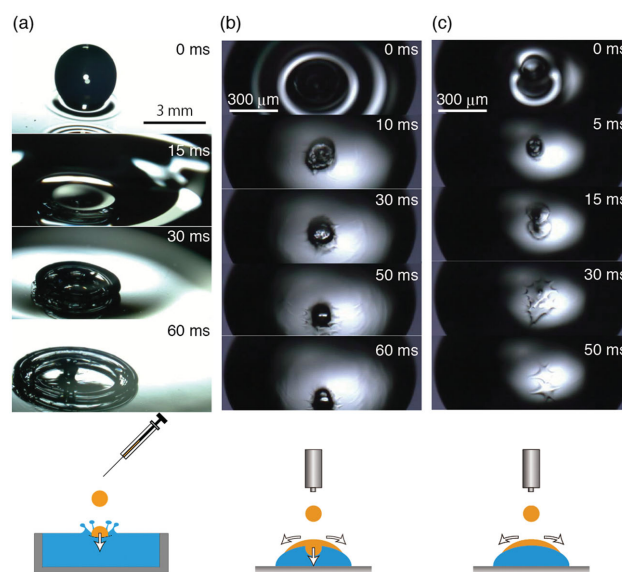


Figure 2. Droplet size effect on the initial contact dynamics of droplet deposition on a chemically different liquid surface. Time-lapse images after the deposition of DCB droplet a) by a micropipette ($\approx 20 \mu\text{L}$), b) an inkjet head ($\approx 1.5 \text{ nL}$), and c) the other inkjet head (0.6 nL) on a surface of DMF. When the volume of the deposited droplet is a) $20 \mu\text{L}$, the initial contact dynamics is governed by a sinking of the deposited droplet due to the density difference (or gravitation), followed by a gradual turbulent or diffusion mixing inside the sessile droplet. By contrast, when the volume of the deposited droplet is c) 0.6 nL , the initial contact dynamics is classified as wetting as reported in this study. The deposition when the volume b) is 1.5 nL is the intermediate case between “gravitation-induced” sinking and wetting.

is the intermediate case between (a) and (c). It is clear that gravity plays no role in droplet deposition for volumes less than 1 nL, where the initial contact dynamics is dominated by advection flow or microdroplet deformation before the start of diffusion mixing.

Next, we focused on the initial mixing dynamics where a microdroplet with volume less than 200 pL is over-deposited on a chemically different sessile droplet of thickness 15–200 μm on a solid surface for various combinations of pure (i.e., without solute) and low-viscous miscible liquids, as presented in Table 1. We observed various types of droplet deformation, depending on the liquid combinations and on the volumes of the sessile droplets. The observed features can be classified into the following three cases:

- 1) Wetting (Figure 3a and Movie S1, Supporting Information): The microdroplet hits the surface of the sessile droplet and spreads over it quickly (within a few milliseconds). The microdroplet is deformed significantly to form a thin liquid layer, while the form of the sessile droplet is temporarily deformed but eventually restored to its original shape. This behavior was observed for the liquid combinations no. 1–5, when the thickness of the sessile droplet was significantly large (Figure S1, Supporting Information). This feature is considered to be desirable in producing thin films of organic semiconductors. If the microdroplet includes a semiconductor molecule as a solute, a thin solution layer can be formed on the surface of the sessile droplet. As a result, a semiconductor thin film can be obtained.
- 2) Dewetting (Figure 3b and Movie S2, Supporting Information): When we decreased the volume of the sessile droplet, a quite different type of behavior was observed. At the deposition point of the microdroplet, a distinct circular inner contact line appeared in the sessile droplet. This contact line expanded quickly within ca. 300 ms to a diameter of about 600 μm , then started to shrink after 400 ms, and eventually disappeared. The dewetting behavior appeared in the same combination of liquids as where the wetting behavior was observed. The transition from wetting to dewetting abruptly occurred with the decrease in the sessile droplet volume. From

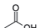
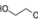
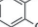





experimental observations detailed later, this behavior was found to appear when the microdroplet touches and spreads over the substrate surface to form a thin liquid layer.

- 3) Sinking (Figure 3c and Movie S3, Supporting Information): For other combinations of liquids, the microdroplet did not stay on the surface of the sessile droplet, but was instead absorbed by the sessile droplet. The microdroplet kept its spherical form and eventually diffused into the sessile droplet. This behavior is clearly different from the two types of behavior described above. It was observed for liquid combinations no. 6–10, and was always detected independent of the volume of the sessile droplet (Figure S2, Supporting Information). The dewetting behavior was not observed even when the microdroplet clearly touched the substrate. The driving force here is thus not gravity. In fact, in combination no. 9, the density of the microdroplet (water, 0.998 g mL^{-1}) was less than that of the sessile droplet (ethylene glycol, 1.11 g mL^{-1}).

Note that the above three kinds of behavior were specifically seen only when the volume of the deposited droplet was small enough (<1.5 nL). We also briefly mention here that the advection flow dominates the molecular diffusion in the present time scale. The microdroplet could spread over a length of $\approx 100\text{--}200\text{ }\mu\text{m}$ after 10 ms, while molecules diffuse only over a length of 1–3 μm during such time (here the diffusion coefficient D is estimated to be $10^{-9}\text{ m}^2\text{ s}^{-1}$ [22]). The Péclet number ($Pe = LU/D$, where L is characteristic length and U is velocity) is also of the order of 1000.

From the classification of behavior for all combinations of liquids, we realized that the difference in surface tension, rather than polarity or density, between the droplets is the primary factor in the initial contact dynamics. Figure 3d presents the initial contact dynamics for a variety of liquid combinations. When the surface tension of the deposited microdroplet is lower than, or almost equal to, that of the sessile droplet (nos. 1–5), dewetting or wetting is observed. By contrast, sinking is observed when the deposited microdroplet has a higher surface tension (nos. 6–10). The results demonstrate that the effect of surface tension is crucial in the appearance of the behaviors that are unique to microdroplets with a length scale less than the capillary length.

Table 1. Parameters of the liquids used in this study.

Liquid (abbreviation)	Molecular structure	Volume per shot [pL]	Velocity [m s^{-1}]	Vapor pressure ^[36,37] [Pa]	Boiling point ^[36,38] [$^{\circ}\text{C}$]	Viscosity ^[38] [mPa s]	Contact angle on SiO_2	Surface tension ^[39] [mN m^{-1}]	Dielectric constant ϵ_r ^[38]
Acetic acid (AA)		146	1.1	1500 (20 $^{\circ}\text{C}$)	118	1.1	0 $^{\circ}$	29.6	6.20
Ethylene glycol (EG)		42	1.4	7 (20 $^{\circ}\text{C}$)	198	16	0 $^{\circ}$	50.2	41.4
1,2-dichloro-benzene (DCB)		22, 600, and 1500	1.9–2.1	160 (20 $^{\circ}\text{C}$)	180	1.3	22 $^{\circ}$	36.9	10.12
<i>N,N</i> -dimethyl-formamide (DMF)		35	2.2	492 (25 $^{\circ}\text{C}$)	153	1.9	0 $^{\circ}$	36.2	38.25
Dimethyl sulfoxide (DMSO)		201	0.67	59 (20 $^{\circ}\text{C}$)	189	1.5	0 $^{\circ}$	42.9	47.2
Tetradecane (TD)		50	4.3	1.5 (20 $^{\circ}\text{C}$)	253	2.1	0 $^{\circ}$	27.6	2.06
<i>N</i> -methylpyrrolidone (NMP)		70	2.0	66 (25 $^{\circ}\text{C}$)	202	1.7	0 $^{\circ}$	41.2	32.2
Ultrapure water (UW)		40–50	1.8–2.0	2330 (20 $^{\circ}\text{C}$)	100	1.0	7 $^{\circ}$	71.9	80.2

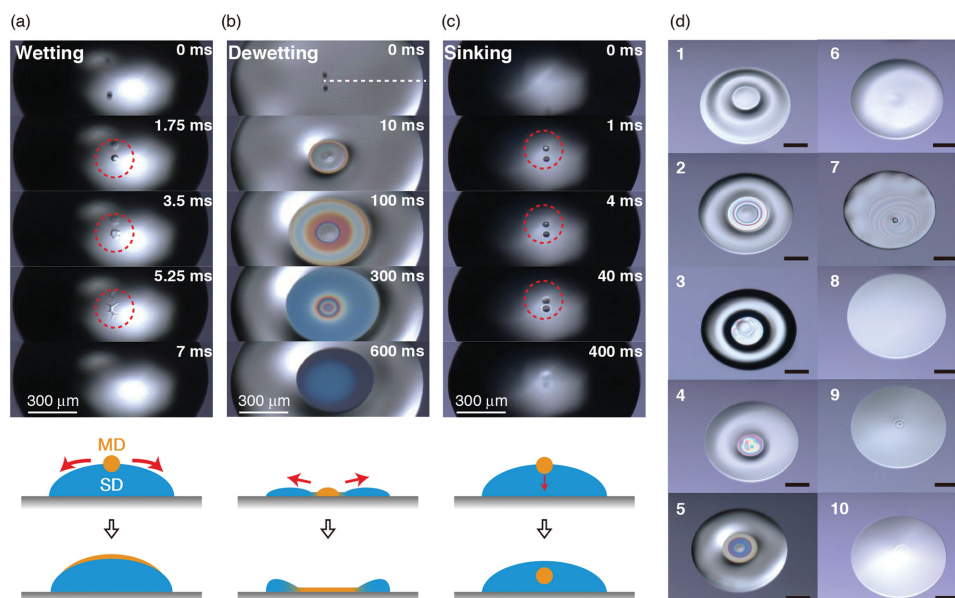


Figure 3. a–c) Typical mixing dynamics of miscible microdroplets. Sequential microscope images of (a) wetting of a 22 pL DCB microdroplet on a 100 nL DMF sessile droplet (Movie S1, Supporting Information), b) dewetting of 22 pL DCB microdroplet on a 10 nL DMF sessile droplet (Movie S2, Supporting Information), and c) sinking of a 47 pL ultrapure water microdroplet in a 100 nL ethylene glycol sessile droplet (Movie S3, Supporting Information), shown with their respective schematic diagrams at the bottom. d) Initial contact dynamics when a microdroplet is deposited on a chemically different sessile droplet for a variety of liquid combinations. A single microdroplet with diameter of $\approx 30\ \mu\text{m}$ is dropped over a surface of sessile droplet with a volume of 10 nL (with height of $16\ \mu\text{m}$ at the center) placed on a circular hydrophilic area with diameter of $1250\ \mu\text{m}$. Snapshots taken 30 ms after microdroplet depositions are shown for all the cases. We find that the wetting–dewetting competition is clearly observed for five miscible combinations (nos. 1–5), whereas sinking is observed for the other five miscible combinations (nos. 6–10). Scale bar is $300\ \mu\text{m}$.

Among the observations, the appearance of dewetting is most extreme, although it is not clear what happens in the dewetted area. To understand this behavior, we present in **Figure 4a** a time evolution of microscope image sequences at the dashed line in **Figure 3b**. On the surface within the dewetted area, we clearly observe the color variation with time due to optical interference. This indicates that a liquid layer is formed by the deposited microdroplet. We also performed interference analyses and plotted the thickness distribution of the liquid layer at different time intervals after microdroplet placement (see **Figure 4b**). The thickness distribution is shaped like a spherical cap to a distance of less than $100\ \mu\text{m}$ from the center, with a thin (less than $100\ \text{nm}$) peripheral layer that touches the inner contact line within the sessile droplet. The thickness in the center decreases rapidly while the thin peripheral layer continues to cover the dewetted area. The peripheral layer is found to be much thinner than $100\ \text{nm}$ at $t > 400\ \text{ms}$, although the exact thickness cannot be estimated using the interference method. The inner contact line starts to shrink after the disappearance of the thicker region at the center. From these observations, we believe that the microdroplet forms an ultrathin ($\ll 100\ \text{nm}$) liquid layer which works as a stable precursor film^[23] that drives the sessile droplet out until the microdroplet disappears, probably through evaporation or diffusion into the sessile droplet. This suggests that the emergence of the solid–liquid interface between the deposited microdroplet and the solid surface is crucial in causing the dewetting behavior.

2.2. Surface Energy Consideration for Initial Contact Dynamics of Microdroplets

Based on the observation as presented in the former section, we can model the wetting, dewetting, and sinking simply in terms of the static energy balance rather than the hydrodynamic analysis^[24] as schematically shown in **Figure 5a**. To discuss the mechanism of these phenomena, we first consider the gain of total surface (or interfacial) free energy by the deformation of the droplets due to the advection flow where the molecular diffusion is neglected. The energy gain, ΔE , can be simply expressed as

$$\Delta E = - \sum_{ij} \gamma_i^j \Delta A_i^j \quad (1)$$

Here, γ_i^j is the surface (interfacial) tension, ΔA_i^j is the change in the interfacial area, subscript i denotes a micro (M) or sessile (S) droplet, superscript j denotes the gas–liquid (gl), solid–liquid (sl), or liquid–liquid (ll) interface. The wetting phenomenon is assumed to be that in which the large gas–liquid surface of the sessile droplet with an area of A_{WET} is covered by the microdroplet (see **Figure 5a**, left). In this case, the energy gain, ΔE_{WET} , can be expressed as

$$\Delta E_{\text{WET}} \equiv (\gamma_S^{\text{gl}} - \gamma_M^{\text{gl}} - \gamma_{\text{SM}}^{\text{ll}}) A_{\text{WET}} \quad (2)$$

Here, we assume that the initial surface area of the microdroplet, denoted as A_M , is much smaller than A_{WET}

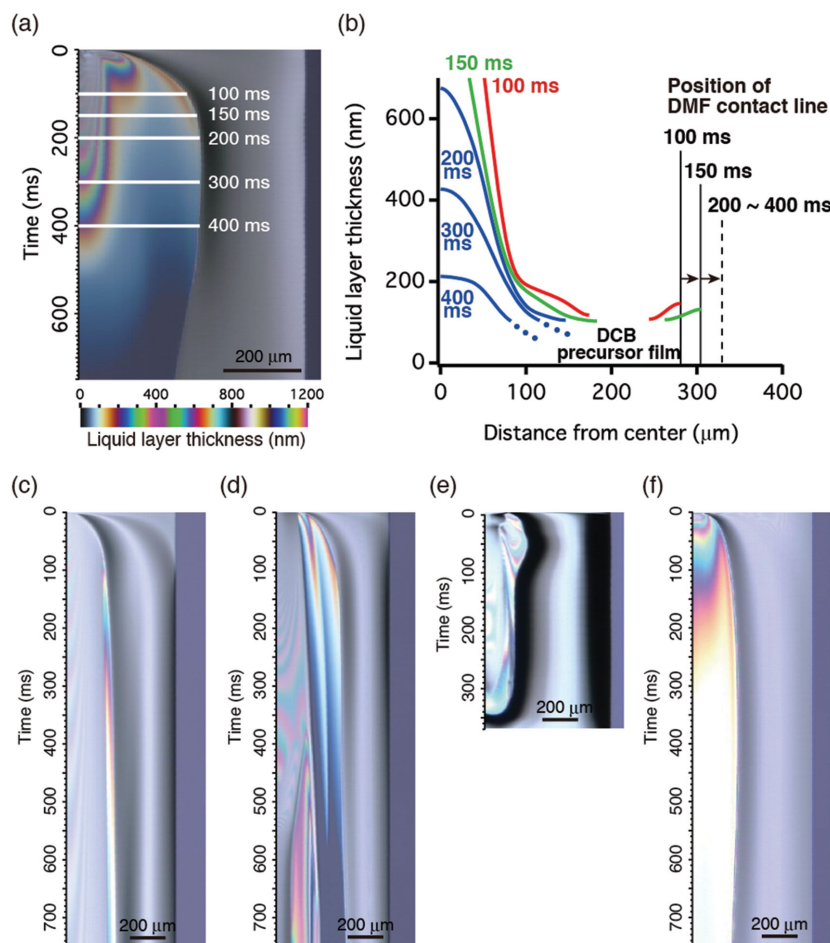


Figure 4. a) Time-lapse image showing the temporal evolution of the dewetting area after deposition of a single DCB microdroplet on a DMF sessile droplet, taken along the white dotted line in Figure 3b. The interference color chart is shown at the bottom. b) Thickness profile of thin liquid layer formed within the dewetted area after different time intervals. c–f) Temporal evolution of dewetting in the case of four miscible liquid combinations. Time-lapse image taken after a single microdroplet deposition on a sessile droplet. c) microdroplet/sessile droplet = tetradecane/ethylene glycol, d) tetradecane/DMF, e) DCB/dimethylsulfoxide, and f) DMF/N-methylpyrrolidone.

($A_M/A_{\text{WET}} \ll 0.1$). Additionally, because the two liquids are miscible, $\gamma_{\text{SM}}^{\text{el}}$ should be almost zero or negative. Eventually, energy is gained due to the wetting if the surface tension of the microdroplet is lower than that of the sessile droplet (i.e., $\gamma_{\text{M}}^{\text{el}} < \gamma_{\text{S}}^{\text{el}}$). For dewetting, the sessile droplet is assumed to be dewetted over an area that we define as A_{DEWET} , which is covered by a thin liquid layer of the microdroplet (see Figure 5a, middle). In this case, the energy gain, ΔE_{DEWET} , can be expressed as

$$\Delta E_{\text{DEWET}} \cong (\gamma_{\text{S}}^{\text{el}} - \gamma_{\text{M}}^{\text{el}} + \gamma_{\text{S}}^{\text{el}} - \gamma_{\text{M}}^{\text{el}}) A_{\text{DEWET}} \quad (3)$$

Here, we assume that the A_{DEWET} is much larger than A_{M} and that the initial form of the sessile droplet surface is flat in the center, such that the changes in the interfacial areas of both sessile droplet and microdroplet are nearly equal to A_{DEWET} . The term $\gamma_{\text{S}}^{\text{el}} - \gamma_{\text{M}}^{\text{el}}$ in Equation (2) is also found in Equation (3). By contrast, when microdroplet with higher surface tension

deposited on sessile droplet with lower surface tension, interfacial energy gain could not be expected, so that the sinking should appear. This surface tension difference is thus the common origin of both the wetting and dewetting phenomena and separates them from the sinking behavior.

To discuss the origin of the sudden transition from the wetting to the dewetting, we plot the appearance of these phenomena at various sizes (i.e., base radius and height) of sessile droplet in Figure 3b for the liquid combination of no. 5 (DCB/DMF). The transition commonly occurs when the center height (thickness) of the sessile droplet, h_{S} , is approximately 50 μm. To understand the behavior, we employed a modified Weber number, $We' = \rho_{\text{M}} v_{\text{M}}^2 d_{\text{M}}^3 / \gamma_{\text{S}} h_{\text{S}}^2$, as a measure of the relative ratio of the inertial energy of the microdroplet (density ρ_{M} , traveling velocity v_{M} , and diameter d_{M}) relative to the deformation energy of the sessile droplet surface to create a conical concave that touches the substrate surface (surface tension γ_{S} and droplet height h_{S}). As seen in Figure 5b, the wetting–dewetting boundary was clearly separated at $We' \cong 1$. We conclude that the absence or presence of microdroplet contact with the bottom substrate surface should cause the wetting or the dewetting, respectively. Here we note that amount of the kinetic energy should only serve to direct the initial contact dynamics toward either wetting or dewetting. Actually, the inertial energy of the DCB microdroplet is estimated at about 50 pJ, while the variation in the gas–liquid surface free energy as a result of the dewetting of the DMF sessile droplet in Figure 4a is estimated at about 11 nJ.

Based on the above argument, we plotted the phase diagrams to classify the initial contact dynamics. Figure 5c plots the locations of the transitions among the three behaviors as a function of the surface-tension difference between the microdroplet and the sessile droplet ($= \gamma_{\text{M}}^{\text{el}} - \gamma_{\text{S}}^{\text{el}}$) and of the We' for all liquid combinations. The separation of the three behaviors in the diagram clearly demonstrates that the above argument on the competition of the initial contact dynamics is reasonable.

2.3. Sign for Peculiar Precursor Film Formation

In the diagram shown in Figure 5c, there observes an exception to the mechanism presented in the former section: The wetting–dewetting competition is observed for the combination of no. 5 (DCB/DMF), although $\gamma_{\text{DCB}}^{\text{el}}$ is almost same as, or slightly higher than $\gamma_{\text{DMF}}^{\text{el}}$. This may indicate that other parameters such as γ^{el} or γ^{el} in Equations (2) and (3) take more important

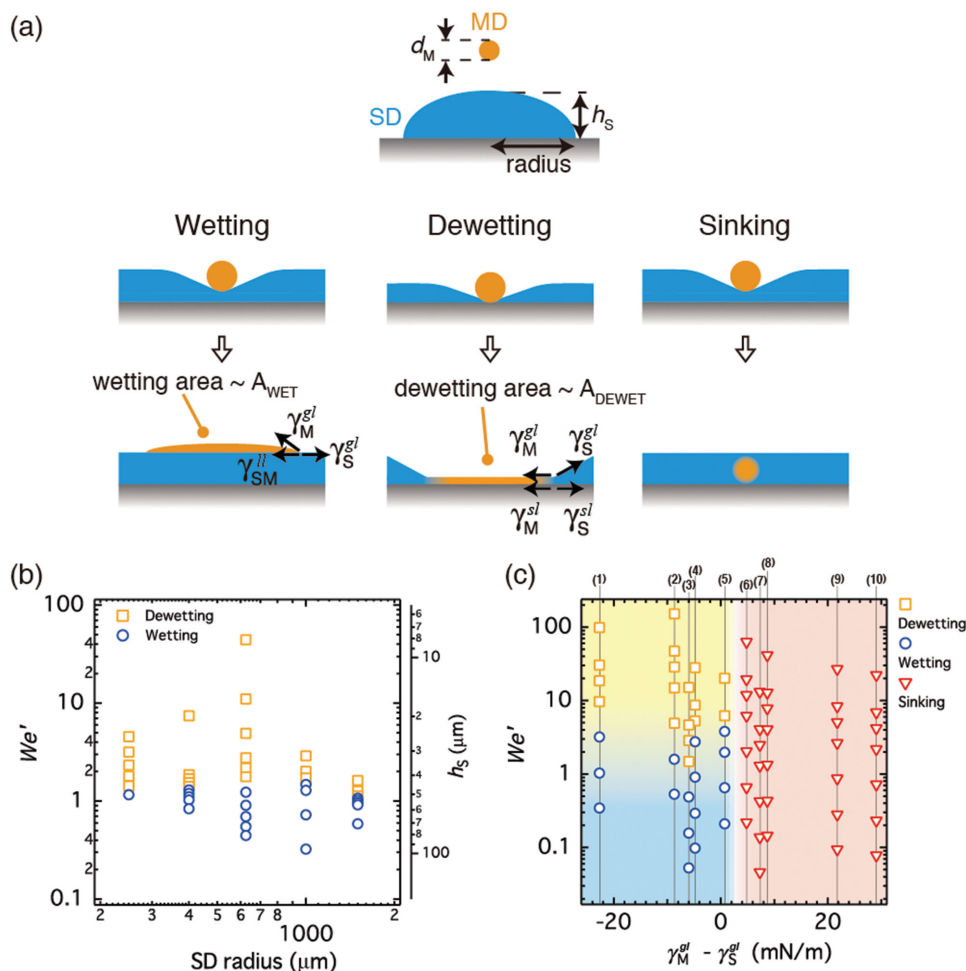


Figure 5. Diagrams showing competition between wetting, dewetting, and sinking. a) Schematic showing balance between interfacial forces in typical mixing dynamics. b) Appearance of wetting or dewetting in the deposition of a DCB microdroplet on a DMF sessile droplet as a function of sessile droplet radius at the liquid–solid interface (transverse axis) and We' number (vertical). c) Wetting, dewetting, or sinking values plotted against the difference in surface tension at the gas–liquid interface ($\gamma_M^{gl} - \gamma_S^{gl}$) (transverse) and the We' number (vertical) for 10 miscible liquid combinations of microdroplets and sessile droplets with regards to the variation in volume of the sessile droplet in a circular hydrophilic area.

roles. However, DCB presents partial wetting characteristics (contact angle $\theta \approx 20^\circ$) in the equilibrium states on the hydrophilic silicon dioxide surface, whereas DMF presents complete wetting ($\theta = 0^\circ$) (see Table 1). This indicates that γ_{DCB}^{sl} must be larger than γ_{DMF}^{sl} according to both the Young's equation ($\gamma^{gl} \cos \theta = \gamma^{sg} - \gamma^{sl}$) and $\gamma_{DCB}^{gl} \approx \gamma_{DMF}^{gl}$, although Equation (3) above describing dewetting phenomenon suggests differently.

We propose that this apparent discrepancy could be understood in terms of the formation of a molecularly thin and stable precursor film^[25–27] of DCB. This supposition is supported by the following observation: We deposited a DCB microdroplet at a position slightly away from a DMF sessile droplet that was confined to a rectangular hydrophilic area, the appearance of which is presented in Figure 6a. It was found that the DCB deposition causes a gradual recession of the contact line of the DMF sessile droplet from the closest corner to the deposition (Movie S4, Supporting Information). A similar observation was recently reported by Tadmor and his co-workers in the combination of acetic acid and water, which they named a “droplet chasing” phenomenon.^[28] The local contact angle^[29] of DMF

sessile droplet after the remote deposition of DCB reached as large as 12° (Figure 6b), whereas γ_{gl} of DMF–DCB mixed liquid was roughly independent of the DCB fraction (Figure 6c). The results indicate that the recession of contact line of the DMF sessile droplet should be ascribed to the decrease of γ_{sg} in the Young's equation, while γ_{gl} was unchanged.^[28,30] This curious behavior could be understood in terms of the precursor-like ultrathin liquid layer formation in the DCB vapour atmosphere on the silicon dioxide surface, as schematically shown in Figure 6d.

We also investigated the spreading speed of a just-deposited DMF sessile droplet with (v') and without (v) the adsorption of the DCB vapor on the substrate surface (Figure 6e). The v' becomes slower than v , indicating that $(\gamma_s^{sl} - \gamma^{sg})$ is increased by the DCB adsorption because of the interfacial force balance as $v \propto -(\gamma_s^{sl} - \gamma^{sg}) - \gamma_s^{gl} \cos \theta_d$ (θ_d is dynamic contact angle).^[31] Note that the presence of DCB did not change the γ_s^{sl} for DMF sessile droplet (Figure 6c). We thus conclude that a DCB ultrathin liquid layer should be formed on the silicon dioxide surface by the DCB vapor adsorption, and should act as a

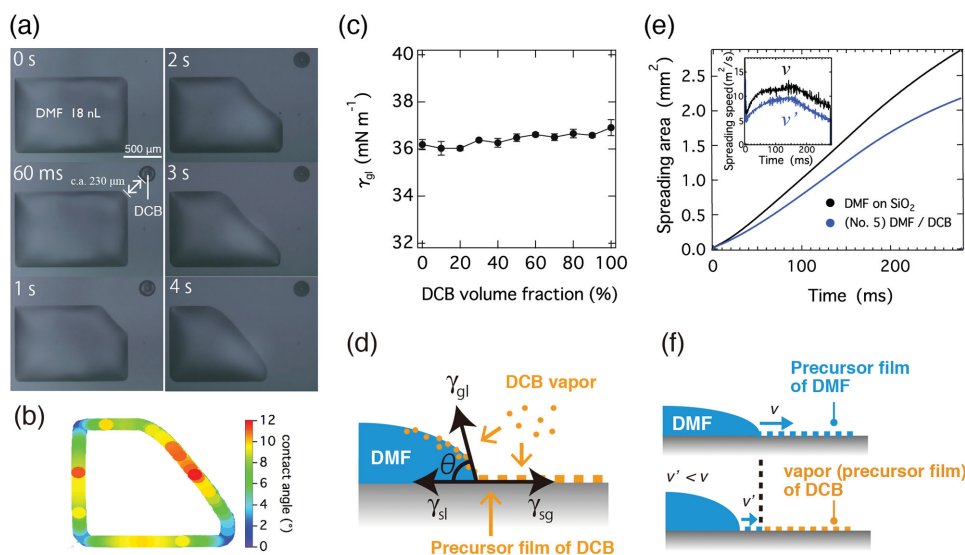


Figure 6. Evidence for precursor film formation by DCB vapor atmosphere on silicon dioxide surface. a) Sequential microscope images for vapor-induced dewetting of a confined DMF sessile droplet (volume of 18 nL) by a DCB microdroplet (volume of 1 nL) deposition at a position slightly away from the confined area (Movie S4, Supporting Information). b) Distribution of local contact angle along the contact line of the DMF sessile droplet 4 s after the DCB microdroplet deposition. c) Surface tension γ_{gl} of DMF–DCB mixed liquids is plotted as a function of DCB volume fraction. d) Scheme of interfacial force balance at the contact line of DMF sessile droplet under the DCB vapor atmosphere. e) Time dependence of the spreading area of the just-deposited DMF droplet on a bare SiO_2 substrate or on a SiO_2 substrate subjected to a saturated DCB vapor atmosphere at least 5 min before the spreading experiment. The DMF droplet volume was constant at 5 nL. Inset: Time dependence of spreading speeds ($\text{m}^2 \text{s}^{-1}$) with (ν') and without (ν) DCB vapor adsorption on a substrate surface. f) Schematic showing the effect of DCB vapor adsorption on spreading speed.

chemically modified surface^[32,33] for the DMF sessile droplet, in spite of the seemingly poor wettability of DCB in the equilibrium state (Figure 6f). We conjecture that the adsorption of DCB vapor should be promoted by, e.g., hydrogen bonds with silicon dioxide surface,^[34] and then the adsorbed layer should behave as a chemically modified surface to affect the wettability of sessile droplets of DMF and of DCB itself. It is interesting to point out that such an adsorbed layer (by DCB molecule) may only be manifested itself through the dewetting phenomenon of another kinds of liquid (of DMF), as demonstrated in the present study. We note that this behavior is clearly different from a similar phenomenon that was observed when two chemically different sessile droplets are placed in close proximity: A sessile droplet chases chemically different sessile droplet, which is induced by the difference of gas–liquid interfacial tension between the droplets.^[19,20]

2.4. Correlation to the Uniform Thin Film Formation

Finally, we demonstrate that the unique initial contact dynamics of binary microdroplets are crucial in the formation of uniform organic semiconductor thin films by the IJP process that adopts a concept of antisolvent crystallization. We used 1 wt% solution of 2,7-dioctyl[1]benzothieno[3,2-b][1] benzothiophene (denoted as C8-BTBT) in DCB as the over-deposited microdroplet and DMF as the antisolvent sessile droplet. **Figure 7** presents a series of microscope images for the entire droplet-mixing phenomena. It was demonstrated that the mixing behaviors are completely changed depending on the volume of DMF sessile droplet.

Figure 7a shows the case of a small volume of sessile droplet, where the over-deposited microdroplet of semiconductor solution causes dewetting of the sessile droplet. Sequential microdroplet deposition with a total volume of a few tens nanoliter causes the independent formation of another sessile droplet of the semiconductor solution that excludes the existing sessile droplet within an interval region of the dewetted area. The respective droplets are time transitional and soon come into contact with each other, which then triggers spontaneous drastic chaotic mixing^[35] between the droplets (Figure 7a and Movies S5 and S6, Supporting Information). As a result, C8-BTBT molecules are present anywhere in the mixed droplet. Mixed droplet starts to form semispherical sessile droplet within the confined rectangular hydrophilic area due to the partial wetting characteristics of DCB (Figure 7a, image at 22 s). At this stage, molecules dissolved in the mixed droplet are easily transported to the area close to the droplet contact line by the outward flow within the droplets. Coffee-ring-like deposits were then eventually formed, through the liquid drying from the mixed droplets in which the microcrystals were precipitated (Figure 7a, image at 144 s).

In striking contrast, when the sessile droplet volume became larger than a certain value, the mixing dynamics presented a sudden change to wetting of DCB microdroplet over the DMF sessile droplet surface. Figure 7b shows a typical example for the case. The droplet form of sessile droplet was unchanged by the microdroplet deposition, whereas the liquid of microdroplet was deformed on the sessile droplet surface (Figure 7b and Movies S7 and S8, Supporting Information). After several tens of seconds, the whole sessile droplet surface became slightly deformed due to the formation of a solid film

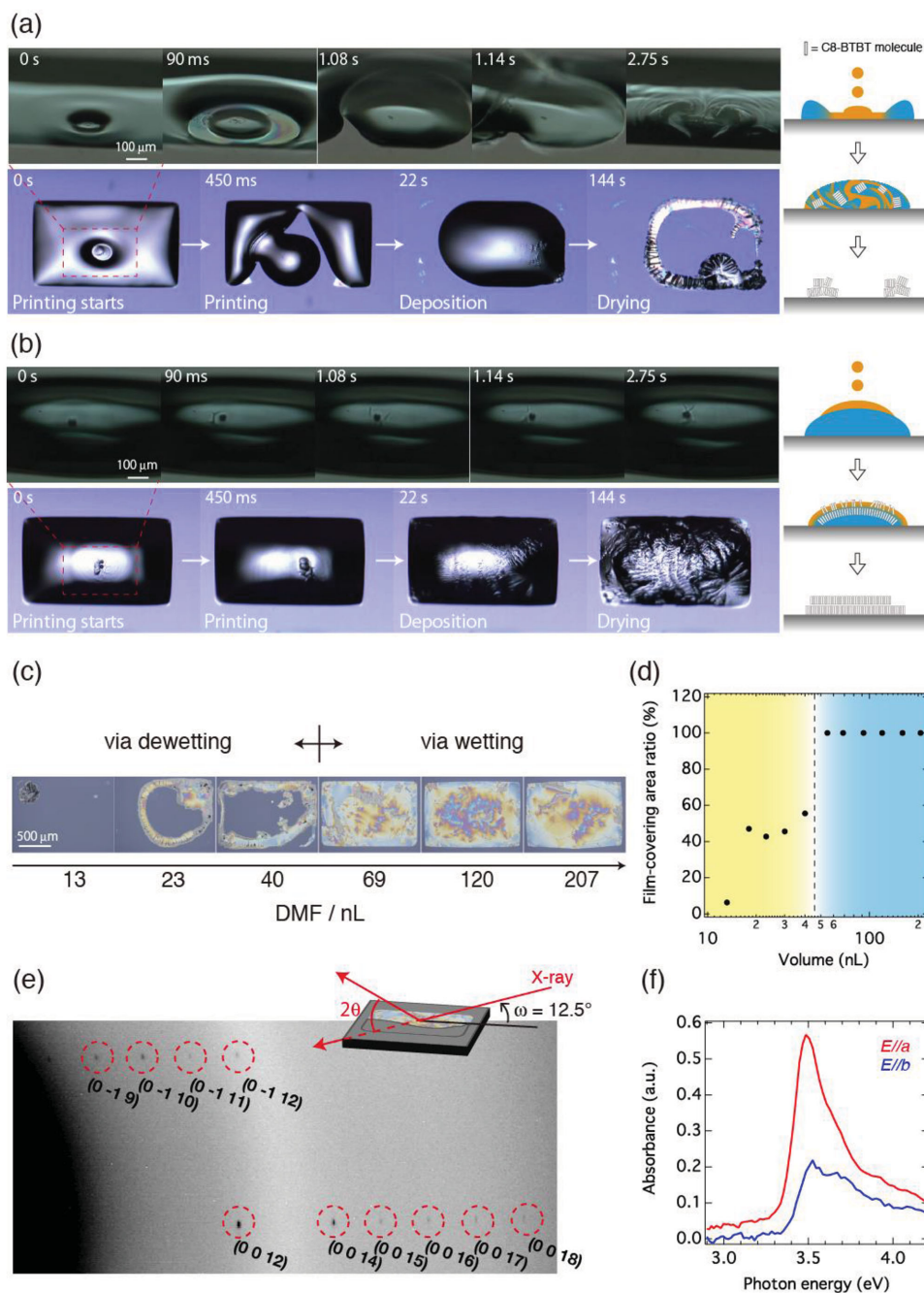


Figure 7. Sequential microscope images (top and bottom views) of material precipitation after a) dewetting of DMF sessile droplet (Movies S5 and S6, Supporting Information) and b) wetting of DMF sessile droplet, both by the deposition of DCB microdroplet (containing 1 wt% C8-BTBT) (Movies S7 and S8, Supporting Information). Schematic of the processes; dewetting causes chaotic mixing, resulting in a coffee ring-like deposit (a, right), and wetting produces a thin solution layer, resulting in a uniform thin film (b, right). c) Effect of initial mixing dynamics on the obtained crystalline thin-film morphology of C8-BTBT. Optical micrographs of C8-BTBT deposits from the same amount of C8-BTBT solution in DCB are shown. d) Film covering area ratio to the predefined hydrophilic area is plotted as a function of DMF sessile droplet volume. e) Synchrotron-radiated X-ray diffraction spectra. Oscillation photographs for out-of-plane diffraction of part of C8-BTBT uniform thin films fabricated by wetting process. ω is the incident angle. f) Polarized absorption spectra with polarization parallel to a and b axes in the film, demonstrating optical anisotropy with regard to these principal axes.

at the liquid–gas interface (Figure 7b, image at 144 s). After liquid drying, a uniform thin film over the area was obtained (Figure 7c). The film-covering area ratio over the predefined hydrophilic area is plotted as a function of the sessile droplet

volume in Figure 7d. It is clear that the sudden change of the covering ratio should be attributed to the transition from the chaotic mixing via dewetting to the thin solution layer formation via wetting. It is thus demonstrated that the use of the

wetting process allows us to produce a thin solution layer on top of the sessile droplet surface, where the gradual diffusion of liquid molecules affords an ideal field for the layered crystalline thin-film formation. Measurements for X-ray diffraction and polarized UV–vis absorption were conducted for the films fabricated by the wetting process, the results of which are shown in Figure 7e,f, respectively. The crystal structure of the obtained C8-BTBT films is identical with the previous report.^[16] Note that the films are composed of a few crystalline domains, because we did not use “bottle-neck-shaped hydrophilic area” for confining the sessile droplet. The observed out-of-plane single-diffraction spots up to 18th order and a clear optical anisotropy in their absorption intensity indicates that the films have a single-crystal domain.

3. Conclusions

We investigated mixing behavior of miscible microdroplets and its effect on subsequent film formation on a solid surface. High-speed camera microscope observations revealed that initial contact dynamics for a microdroplet deposition on a chemically different but miscible sessile droplet can be classified into three types: Fluid dynamic competition between 1) wetting and 2) dewetting is observed when a lower-surface-tension microdroplet is deposited, and 3) sinking appeared when a higher-surface-tension microdroplet is deposited. The main driving force for these behaviors is the surface tension of liquids, which becomes crucial for understanding the initial contact dynamics of the microdroplets. The wetting and dewetting regimes appear when a microdroplet induces a gain of interfacial energy, i.e., the microdroplet covers the sessile droplet surface otherwise it wets on the solid surface. Meanwhile, the sudden transition between wetting and dewetting is triggered by whether the microdroplet contacts on the solid surface or not. The physics of the wetting–dewetting competition is quite useful for manipulating microdroplet dynamics: when organic semiconductor solutions are employed as microdroplet, the wetting process allows us to produce semiconductor thin films. Such an innovative method should lead to the development of emerging print-production technologies for microelectronic devices.

4. Experimental Section

Substrate Treatment: We used silicon substrates with 100 nm thick thermally grown silica layers for the microscope observation from the front side and transparent silica (SiO₂) substrates for the observation from the backside. A combination of surface chemical modification using hexamethyldisilazane (HMDS) and masked UV/O₃ treatments is adopted in order to generate hydrophilic/hydrophobic patterning on the silica surfaces. The substrates were exposed to HMDS vapor for 7 days at room temperature. Then, UV/O₃ treatment was applied again for 15 min through metal shadow masks (SUS430) with circular openings of different diameters (500–3000 μm) or rectangular openings (1000 μm × 1500 μm) in order to restore hydrophilic silanol groups on the surface of the unmasked area. The cleaned substrates were soon used for the experiments to avoid increasing the loss of wettability in ambient atmosphere.^[29]

Microdroplet Deposition: A sessile droplet (with volume between 10 and 180 nL) was first produced on a substrate, and then a microdroplet (with volume of few tens pL) was deposited on the sessile droplet. The subsequent dynamics was observed by a high speed camera. The ten combinations of microdroplet/sessile droplet were 1) tetradecane/ethylene glycol, 2) tetradecane/*N,N*-dimethylformamide (DMF), 3) 1,2-dichlorobenzene (DCB)/dimethylsulfoxide, 4) DMF/*N*-methylpyrrolidone, 5) DCB/DMF, 6) *N*-methylpyrrolidone/DMF, 7) DCB/acetic acid, 8) DMF/tetradecane, 9) ultrapure water/ethylene glycol, and 10) ultrapure water/dimethylsulfoxide (see Figure 1a). Physical parameters of these liquids are listed in Table 1. Prior to the microdroplet deposition, the sessile droplet was confined within circular-shaped hydrophilic area with diameter of 1250 μm surrounded by hydrophobic area.

Deposition of Semiconductor Solution: In the fabrication of organic semiconductor solution, a filtered solution (28×10^{-3} M, 1 wt%) of C8-BTBT in DCB was used. Microdroplets of the semiconductor solution with volumes of a few tens of picoliters were shot continuously at 500 Hz at the centre of the sessile droplet with volume of 13–207 nL reserved in a rectangular hydrophilic area until the total volume reached 2–65 nL. The surface tension of DMF was not affected by the addition of a solute.

High-Speed Camera Microscope Observation: The mixing phenomena and the spreading characteristics of the microdroplets were investigated in situ by a digital high-speed camera (4000 frame s⁻¹ at maximum) microscope (Keyence, VV-9000) equipped with a long-working-distance (85 mm) objective lens with a high magnifying power (×150) (VH-Z50L/Z50W). The observation was viewed by an elevation angle of 60° from the front side. In Figure 6, the experiments were conducted and analyzed on the basis of backside observations. In order to investigate the vapor effect (Figure 6e, shown in blue), the SiO₂ substrates were subjected to a saturated vapor atmosphere of DCB at least 3 min before the spreading experiment.

Film Characterization: The synchrotron radiated X-ray measurements were conducted at the BL-8B line of the KEK (High Energy Accelerator Research Organization) Photon Factory. The X-rays that were used had an energy of 18 keV (wavelength 0.6776 Å). The monochromated beam was focused at the sample position with beam size of 300 μm × 300 μm. The oscillation photographs were taken at Δω = 5°. A Cassegrain-type microscope combined with a grating monochromator (JASCO MSV-370) was used to measure the anisotropic optical absorption spectra.

Supporting Information

Supporting Information is available from the Wiley Online Library or from the author.

Acknowledgements

The authors are grateful to Yasushi Hori (Microjet, Japan) for his help in constructing the experimental setup for high-speed camera microscope observation of microdroplet depositions. The authors are also grateful to Nippon Kayaku for providing C₈-BTBT. This work was partly supported by the NEDO through a Grant for Industrial Technology Research, by the JST through a CREST project, and also by the JSPS KAKENHI Grant No. 26246014.

Received: February 28, 2015

Revised: April 18, 2015

Published online: May 18, 2015

- [1] W. Smaal, C. Kjellander, Y. Jeong, A. Tripathi, B. van der Putten, A. Facchetti, H. Yan, J. Quinn, J. Anthony, K. Myny, W. Dehaene, G. Gelinck, *Org. Electron.* **2012**, *13*, 1686.

- [2] K.-J. Baeg, S.-W. Jung, D. Khim, J. Kim, D.-Y. Kim, J. B. Koo, J. R. Quinn, A. Facchetti, I.-K. You, Y.-Y. Noh, *Org. Electron.* **2013**, *14*, 1407.
- [3] X. Cheng, M. Caironi, Y.-Y. Noh, C. Newman, J. Wang, M. J. Lee, K. Banger, R. Di Pietro, A. Facchetti, H. Sirringhaus, *Org. Electron.* **2012**, *13*, 320.
- [4] T. N. Ng, S. Sambandan, R. Lujan, A. C. Arias, C. R. Newman, H. Yan, A. Facchetti, *App. Phys. Lett.* **2009**, *94*, 233307.
- [5] H. Yan, Z. Chen, Y. Zheng, C. Newman, J. R. Quinn, F. Dotz, M. Kastler, A. Facchetti, *Nature* **2009**, *457*, 679.
- [6] D. Tobjork, R. Osterbacka, *Adv. Mater.* **2011**, *23*, 1935.
- [7] R. D. Deegan, O. Bakajin, T. F. Dupont, G. Huber, S. R. Nagel, T. A. Witten, *Nature* **1997**, *389*, 827.
- [8] J. A. Lim, W. H. Lee, H. S. Lee, J. H. Lee, Y. D. Park, K. Cho, *Adv. Funct. Mater.* **2008**, *18*, 229.
- [9] M. Singh, H. M. Haverinen, P. Dhagat, G. E. Jabbour, *Adv. Mater.* **2010**, *22*, 673.
- [10] W. Sempels, R. De Dier, H. Mizuno, J. Hofkens, J. Vermant, *Nat. Commun.* **2013**, *4*, 1757.
- [11] T. Kajiyama, W. Kobayashi, T. Okuzono, M. Doi, *Langmuir* **2010**, *26*, 10429.
- [12] T. Kajiyama, W. Kobayashi, T. Okuzono, M. Doi, *J. Phys. Chem. B* **2009**, *113*, 15460.
- [13] P. J. Yunker, T. Still, M. A. Lohr, A. G. Yodh, *Nature* **2011**, *476*, 308.
- [14] D. Soltman, V. Subramanian, *Langmuir* **2008**, *24*, 2224.
- [15] R. Bhardwaj, X. Fang, P. Somasundaran, D. Attinger, *Langmuir* **2010**, *26*, 7833.
- [16] H. Minemawari, T. Yamada, H. Matsui, J. Tsutsumi, S. Haas, R. Chiba, R. Kumai, T. Hasegawa, *Nature* **2011**, *475*, 364.
- [17] H. H. Tung, E. L. Paul, M. Midler, J. A. McCauley, *Crystallization of Organic Compounds: An Industrial Perspective*, Wiley-AlChE, New York, **2009**, pp 179–205.
- [18] J. Atencia, D. J. Beebe, *Nature* **2005**, *437*, 648.
- [19] S. Karpitschka, H. Riegler, *Phys. Rev. Lett.* **2012**, *109*, 066103.
- [20] R. Borcia, M. Bestehorn, *Langmuir* **2013**, *29*, 4426.
- [21] R. Yerushalmi-Rozen, T. Kerle, J. Klein, *Science* **1999**, *285*, 1254.
- [22] J. Wang, T. Hou, *J. Comput. Chem.* **2011**, *32*, 3505.
- [23] A. Hoang, H. P. Kavehpour, *Phys. Rev. Lett.* **2011**, *106*, 254501.
- [24] S. T. Thoroddsen, B. Qian, T. G. Etoh, K. Takehara, *Phys. Fluids* **2007**, *19*, 072110.
- [25] M. N. Popescu, G. Oshanin, S. Dietrich, A. M. Cazabat, *J. Phys. Condens Matter.* **2012**, *24*, 243102.
- [26] F. Tiberg, A. M. Cazabat, *Langmuir* **1994**, *10*, 2301.
- [27] D. R. Heine, G. S. Grest, E. B. Webb, *Phys. Rev. Lett.* **2005**, *95*, 107801.
- [28] P. Bahadur, P. S. Yadav, K. Chaurasia, A. Leh, R. Tadmor, *J. Colloid Interface Sci.* **2009**, *332*, 455.
- [29] Y. Noda, H. Matsui, H. Minemawari, T. Yamada, T. Hasegawa, *J. App. Phys.* **2013**, *114*, 044905.
- [30] M. K. Chaudhury, G. M. Whitesides, *Science* **1992**, *256*, 1539.
- [31] P. G. de Gennes, F. Brochard-Wyart, D. Quere, *Capillarity and Wetting Phenomena: Drops, Bubbles, Pearls, Waves*, Springer, New York **2004**.
- [32] S. C. Hernandez, C. J. C. Bennett, C. E. Junkermeier, S. D. Tsoi, F. J. Bezares, R. Stine, J. T. Robinson, E. H. Lock, D. R. Boris, B. D. Pate, J. D. Caldwell, T. L. Reinecke, P. E. Sheehan, S. G. Walton, *ACS Nano* **2013**, *7*, 4746.
- [33] O. Bliznyuk, H. P. Jansen, E. S. Kooij, H. J. W. Zandvliet, B. Poelsema, *Langmuir* **2011**, *27*, 11238.
- [34] N. Giovambattista, P. G. Debenedetti, P. J. Rossky, *J. Phys. Chem. B* **2007**, *111*, 9581.
- [35] M. R. Bringer, C. J. Gerdt, H. Song, J. D. Tice, R. F. Ismagilov, *Philos. Trans. R. Soc. London Ser. A* **2004**, *362*, 1087.
- [36] The International Chemical Safety Cards (ICSC) database.
- [37] T. E. Daubert, R. P. Danner, *Physical & Thermodynamic Properties of Pure Chemicals*, Taylor & Francis, London **1992**.
- [38] J. G. Speight, *Lange's Handbook of Chemistry*, 16th ed., McGraw-Hill Professional, New York **2005**.
- [39] Surface tension was measured by using Wilhelmy method at 20 °C.